Articles   School of Civil and Structural Engineering

2020-08-27

The use of three-dimensional conjugate CFD to enhance understanding of, and to verify, multi-modal heat transfer in dynamic laboratory test walls

Rakshit D. Muddu
Technological University Dublin, d16126147@mytudublin.ie

Timothy Patrick O'Leary
Technological University Dublin, timothy.oleary@tudublin.ie

Ronan Hogan
Technological University Dublin, ronan.hogan@tudublin.ie

See next page for additional authors
Follow this and additional works at: https://arrow.tudublin.ie/engschcivart

Part of the Civil and Environmental Engineering Commons

Recommended Citation

Authors

Rakshit D. Muddu, Timothy Patrick O'Leary, Ronan Hogan, Anthony James Robinson, and Aimee Byrne

The use of three-dimensional conjugate CFD to enhance understanding of, and to verify, multi-modal heat transfer in dynamic laboratory test walls

Rakshit D M[1] , Tim O'Leary[2], Ronan Hogan[3], Anthony James Robinson[4] , Aimee Byrne[1]

[1]Department of Civil& Structural Engineering, Technological University, Dublin, Ireland,
[2]Dublin School of Architecture, Technological University, Dublin, Ireland,
[3]Surveying and construction management, Technological University, Dublin, Ireland
[4]Department of Mechanical and Manufacturing Engineering, Trinity College Dublin, Dublin, Ireland
email: D16126147@mytudublin.ie, timothy.oleary@TUDublin.ie, ronan.hogan@TUDublin.ie, arobins@tcd.ie,
aimee.byrne@TUDublin.ie

ABSTRACT: This work describes the use of conjugate computational fluid dynamics (C-CFD) to simulate controlled laboratory based dynamic heat transfer tests on building components. This study proposes that conjugate CFD simulation can be used to evaluate the influence of combined convective and conductive heat transfer in multi-state building components. To this end, a solid wall and cavity wall were tested with a Calibrated Hotbox and subject to variable temperature conditions leading to combined convective and conductive heat transfer. The varying temperature of the heat source was monitored and used as the input boundary condition in the simulation model, which included a computational domain which encompassed the hot-side air chamber and the wall, including cavity when applicable. It was found acceptable accuracy could be realized with a simplified constant surface heat transfer coefficient with fixed air temperature on the cold air side, which greatly reduced computational effort. The experimental results revealed that the cavity wall experienced a phase lag, peak displacement of 2.9 times higher and decrement factor 1.6 times lower compared with that of the solid wall.

KEY WORDS: Calibrated Hotbox; Heat Transfer; Phase Lag; Decrement Factor; C-CFD Simulation.

1 INTRODUCTION

Globally, the building sector is the second largest consumer of energy, accounting for approximately 40% of energy consumption [1]. This implies that a reduction in energy consumption for heating and cooling in buildings would contribute significantly to achieving sustainability goals. Concerning this, many engineers worldwide adopt an energy saving approach when designing the building envelope. However, many building codes primarily focus on the thermal transmittance value alone, which excludes the effect of thermal mass [2].

Envelopes with high thermal mass can absorb and store heat during the heating period and progressively release the stored heat back to the immediate environment during the non-heating period [3, 4]. This behaviour aids in stabilising indoor temperature and reducing the heating demand while maintaining occupant comfort.

Phase lag (or time lag) and decrement factor are thermal performance parameters of materials under transient conditions. When a sinusoidal heat wave moves from the hot to cold side, the amplitude of the wave reduces. The reduction ratio in amplitude between the two surfaces is called the *decrement factor*. The position of the peak temperature is displaced as it moves through the wall in what is termed the *peak displacement* and the associated time shift is called phase lag. Many studies have investigated what influences time lag and decrement factor [5-7]. These factors are profoundly influenced by thickness of the section and the effective thermal diffusivity (α) [5, 6]. Balaji et al. [6] identified that extrinsic properties, such as surface heat transfer coefficients, were of little influence on these parameters. Walls with a higher time lag and lower decrement factors maintain a more stable indoor temperature [6]. Therefore, some studies [8, 9] have focused on

their relationship with heating or cooling energy usage and thermal mass placement [9-11] or wall orientation [12, 13]. The results of these studies reveal that east facing walls with external insulation experience maximum time lag and decrement factor.

Few experimental studies have been conducted on these important parameters. One study used the parameters to determine the influence of thermal inertia [14]. When wall configurations are compared experimentally, results showed that multi-layered walls performed well compared to the single-layered or thin walls [15, 16] which agrees with the numerical studies. In the majority numerical studies performed, time lag and decrement factors have been investigated based on one-dimensional finite difference methods with very few supporting experiments [17, 18]. Further, the influence of natural convection in the cavities were neglected by assuming purely conductive heat transfer through the cavity, which is not always a valid assumption[19].

Due to the different material properties of wall components depending on manufacturer, time lag and decrement factor will differ between countries. Irish housing is recognised as amongst the least energy efficient in Northern Europe [20]. Therefore, by evaluating the thermal performance walls made from locally available materials, this work contributes knowledge to the field of building energy efficiency.

The objective of this work is to investigate the dynamic thermal behaviour of a solid wall and a cavity wall experimentally and compare the results with numerical simulation.
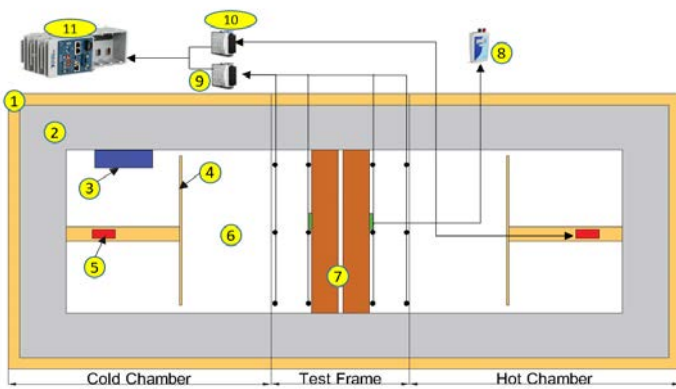
1	45mm Iberpan 400	8	Hukse Flux data logger
	200 mm EPS	9	NI-Module for temperature
3	Chiller unit		data logging
4	Baffle	10	NI-Module for temperature
5	Heating unit		control
6	Air HC or CC	11	Compact RIO DAQ chassis
7	Sample walls		

Figure 2.Schematic representation of the Hotbox components

2 EXPERIMENTAL METHODOLOGY

2.1 Hotbox

A schematic representation of the Calibrated Hotbox at Dublin Energy Lab (DEL) is shown in Figure 1. The Hotbox comprises of a Hot Chamber (HC) (1.2m x 1.2m x 1.2m), Test Frame (TF) (0.6m x 1.2m x 1.2m) and a Cold Chamber (CC) (1.2m x 1.2m x 1.2m). The test frame hosts a test specimen of size 0.715m X 0.715m and thickness of up to 0.6 m. The TF holding the specimen is sandwiched between the HC and CC, separating the chambers.

2.1.1 Heating and cooling

An anti-condensation heating unit heats the HC from behind the baffles to avoid the influence of the radiation directly on to the test specimen (Figure 1). Using PID control system, the heating unit can be switched on and off periodically to create transient conditions or to maintain a constant air temperature.

The CC is equipped with an air-cooled refrigerator, mounted behind a baffle panel (Figure 1). The refrigerator's evaporator cools the air directly inside the CC. The operating temperature of the CC is set manually through the digital thermostat. The CC is also equipped with a heating unit in order to control temperature undershoot.

2.1.2 Measurements and data acquisition

K-type thermocouples are used to measure surface and air temperatures to an accuracy ±0.75%. As depicted in Figure 1 and Figure 2, a total of 16 were used; four on CC side, eight on HC side and four inside the cavity of the cavity wall. They were connected to an NI Compact DAQ system in conjunction with LabView. Additionally, two HFP01 heat flux sensor plates, with accuracy ±3%, were placed on the hot and cold side surfaces of the test specimens connected to an LI19 datalogger to record the heat flux into and from the wall.
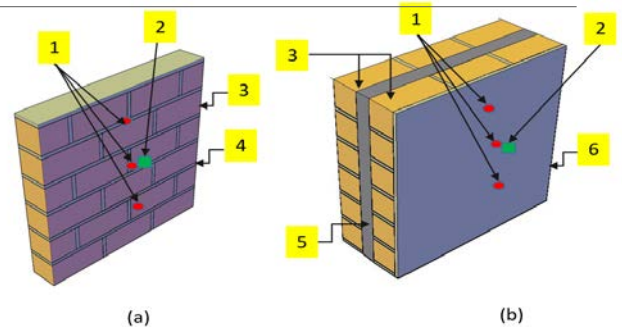
1	Thermocouple	4	Mortar joints
2	Heat flux sensor	5	Cavity layer (air)
3	Brick layer/s	6	Plaster layer

Figure 1. (a-b) Locations of sensors on the (a) solid wall & (b) cavity wall

2.2 Laboratory test

Figure 2(a-b) shows the structural configurations of the walls and representative location of sensors. Thermocouples and heat flux meters were set to record at 30s and 300s intervals respectively. The temperature of the CC was maintained at a constant low temperature set-point of 5 °C and the HC air temperature set to vary sinusoidally over a time span of 24 hours between T_{max} = 30° C and T_{min} = 20° C. The HC heater unit operates under two-phases during testing, namely the linear heat- up phase followed by sine wave heating. During the linear phase, the temperature in the HC continuously rises until it reaches the desired set-point, after which the sinusoidal phase is initiated which undulates with respect to this set-point.

3 EVALUATION OF THERMODYNAMIC PARAMETERS

Data from the thermocouples and heat flux meters positioned as shown in Figure 1 and Figure 2 were recorded over several days. Two days of recording, which represents two sine wave cycles were chosen for analysis for walls with properties listed in Table 1.

Table 1. Thermal properties of wall materials [2]

Material	k (W/m.K)	ρ (kg/m³)	c (J/kg.K)
Brick	0.63	1800	900
Plaster/mortar	0.52	1300	840

3.1 Thermal impedance

Thermal impedance (Z_d) is the temperature gradient per unit of heat flux passing through the wall;

$$Z_d = \int_{0hr}^{24hr} \frac{\Delta T}{q_i} \, dt \qquad (1)$$

where $\Delta T = T_i - T_e$ and q_i is the hot side heat flux.

3.2 Phase lag, peak displacement and decrement factor

Phase lag (∅) and decrement factor (D) and peak displacement (∅d), are determined under dynamic conditions as;

$$D = \frac{Ti, max - Ti, min}{Te, max - Te, min} \qquad (2)$$

$$\emptyset = t(Ti, max - Te, max) \tag{3}$$

$$\emptyset = t(Ti, min - Te, min) \tag{4}$$

$$\emptyset d = t(Ti, max - Te, max) * 2\sqrt{(\Pi\alpha/P)} \tag{5}$$

where subscript i denotes the hot side, e the cold side and the term $2\sqrt{(\Pi\alpha/P)}$ represent the velocity of the sine wave, P period.
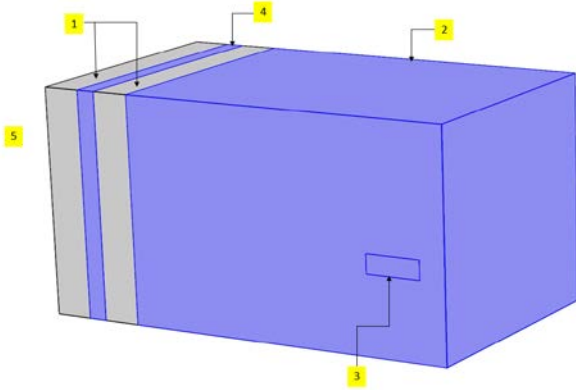

Figure 3. Computational geometry

1	Brick layer	4	Air domain in the cavity wall
2	Air domain in the HC	5	Wall facing the constant 5 °C cold air
3	Heat source		

4   NUMERICAL MODEL

Two numerical models were developed, one for the solid wall and one for the cavity wall. The computational domain is depicted in Figure 3. These models assume constant thermal properties of each material and that the thermal contact resistance between the materials is negligible. The model domain consists of a heater source in the HC, the HC air and the wall sample.

4.1   Governing Equations

The Navier-Stokes equations were used to model the behaviour of laminar flow in the HC,

$$\frac{\partial\rho}{\partial t} + \nabla(\rho u) = 0 \tag{6}$$

$$\rho\frac{\partial u}{\partial t} + \rho(u.\nabla)u = \nabla\left[-p + \mu\left(\nabla u + (\nabla.u)^T\right) - \frac{2}{3}\mu(\nabla.u)\right] + \rho g \tag{7}$$

where p is pressure and μ is dynamic viscosity. The temperature field in the air (f) domain was determined by simultaneously solving the energy equation,

$$\rho c\frac{\partial T_f}{\partial t} + \rho cu.\nabla T_f = \nabla.(k_f\nabla T_f) \tag{8}$$

The heat transfer in the solid domain is dominated by conduction and hence Fourier's law,

$$\rho c\frac{\partial T_s}{\partial t} = \nabla.(-k_s\nabla T_s) \tag{9}$$

4.2   Boundary condition

The input for the modelled HC is the smoothed experimentally monitored temperature of the heating source (Figure 4) as the inlet boundary whereas Newton's law of cooling is used at the cold side surface,

$$-n.q = h.(T_{a-}T_f) \tag{10}$$

Here, h (W/m² K) is the heat transfer coefficient, T_f is a constant 5° C and T_a refers to the surface temperature of the wall. The remaining exposed surfaces of the HC and testing frame are considered to be adiabatic. Initially the air velocity of the fluid was assumed to be zero, and no slip condition (u=0) was assumed at all fluid boundaries.
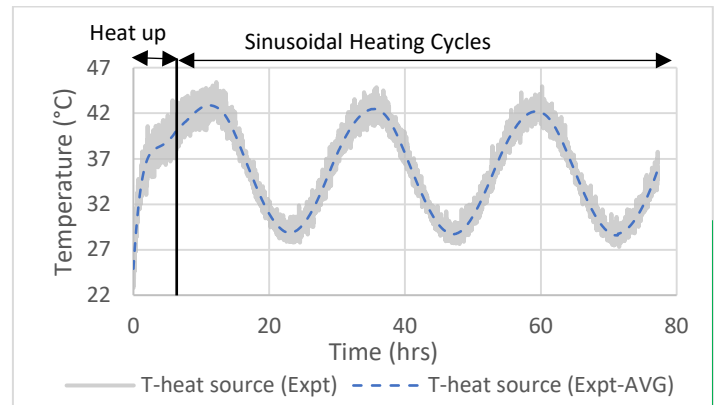

Figure 4. Example of monitored and smoothed temperature of the heat source

5   MODEL EVALUATION INDEX

To assess the capability of the developed simulation model to reproduce the behavior of the experimental wall, the coefficient of variation (CV) and model efficiency (EF) was calculated. The coefficient of variation defines how well the model fits the experimental data by using offsetting errors between measured and simulated output. As per ASHRAE guideline 14 [21], the model is said to be calibrated if the CV of hourly data lies between the value of ± 30 %. This index is given by Eq. 11 where N is the number of samples, E is experimental output and S is simulated output.

$$CV = \frac{\sqrt{\sum_{j=1}^{m}(E_j - S_j)^2/N}}{E_{avg}} \tag{11}$$

The Efficiency factor (EF) [22] compares the efficiency of the simulation model and the efficiency of describing the data as the mean of the experimental observations. This index is given by Eq. 12 and maximum value of 1 is achieved for identical simulation and experimental results.

$$EF = \frac{\sum_{1}^{m}(E_j - E_{avg})^2 - \sum_{1}^{m}(S_j - E_j)^2}{\sum_{1}^{m}(E_j - E_{avg})^2} \tag{12}$$

6   RESULTS AND DISCUSSION

6.1   *Experimental results*

The dynamic analysis of the two sample walls produced very different results for the same applied conditions. The first 3 days of both wall samples is shown in Figure 5 which plot the surface temperatures measured on both hot side and cold sides. Figure 5b also includes the temperature measurement of the air inside the cavity. In each graph, the damping effect thermal mass can be identified by the reduced amplitude of the wave as it moves across the wall from the hot to cold side. The degree of damping is discussed in terms of quantifiable thermodynamic parameters of phase lag, decrement factor and peak displacement, as calculated using the Eqs. (2-5) and summarised in Table 2. It is clear that the cavity wall has larger phase lag and peak displacement with smaller decrement factor. This is because the cavity wall contains additional air and solid layers leading to increased effective thermal mass. Phase lag and decrement factor also depend on the dimensionless parameter $\sqrt{(L^2/P.\alpha)}$ [23] where L is thickness (m) and P (s) is the time period required to complete one cycle, which here is the same for both tests. The cavity wall has a greater total thickness compared to the solid wall, and the air layer acts as an insulator leading to greater phase lag, peak displacement and lower decrement factor. For the walls experiencing smaller phase lag and larger decrement factor, heat loss will be larger [6]. This is clear considering Figure 6, which shows the measured a notably lower average heat flux for the cavity wall. As expected, the thermal impedance was greater for the cavity wall (0.66 K.m^2/W) which resulted in a lower heat loss when compared with the wall solid wall (0.37 K.m^2/W). It can be seen in Figure 6 and Table 2 that the occurrence of the peak heat load is delayed by approximately 4.5 hours when compared to solid wall, illustrating larger thermal mass.
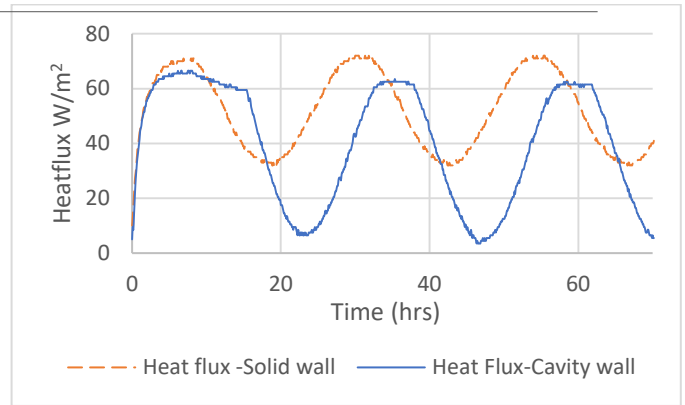

Figure 6. Measured surface heat flux

Table 2. Dynamic parameters – Experiment

	Solid wall	Cavity wall
Ø (hrs)	2.58	6.88
Ød (cm)	0.21	0.62
D (-)	0.32	0.2

6.2   *Verification of the heat transfer simulation*

Figure 7 to Figure 10 compare measured and simulated surface temperatures and heat fluxes for both walls. In the case of the solid wall, the temperature (Figure 7) and heat flux (Figure 8) fluctuations indicated an average relative error of 2.5% and 4% respectively. Particularly good agreement was found for the hot side measurements while on the cold side, a difference of approximately 0.9 K is noted in the crest of the surface temperature plot. These differences are attributed to the unknown and/or assumed surface thermal properties such as convective and radiative heat transfer coefficients, and the assumed constant material properties in the simulation. The variable and case specific nature of heat transfer coefficients found by calculation, experiment and simulation is discussed extensively by Byrne et al. [24].
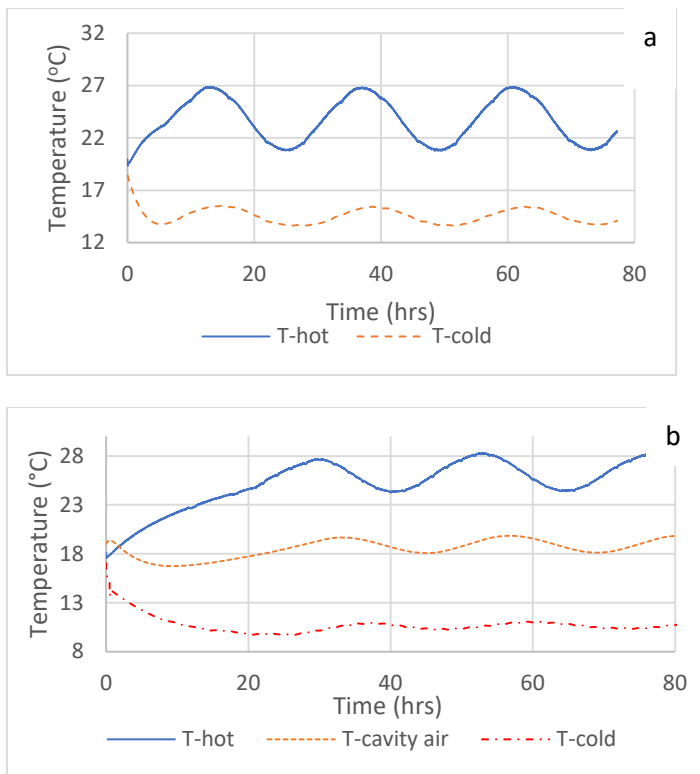

Figure 5. Measured wall surface temperatures of (a) solid wall (b) cavity wall (including cavity air temperature)
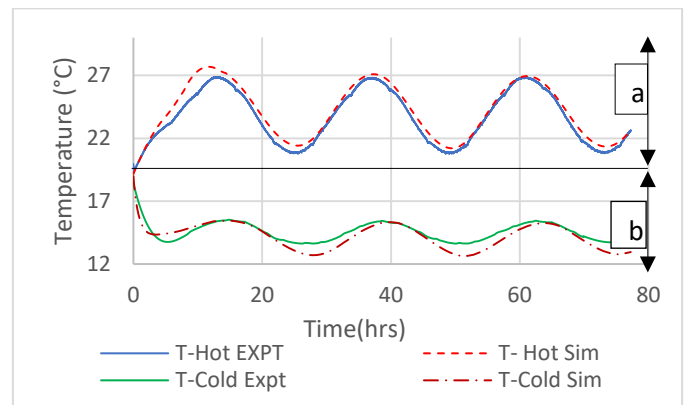

Figure 7. Comparison of experiment and simulations for solid wall data (a) hot side surface temperature (b) cold side surface temperatures
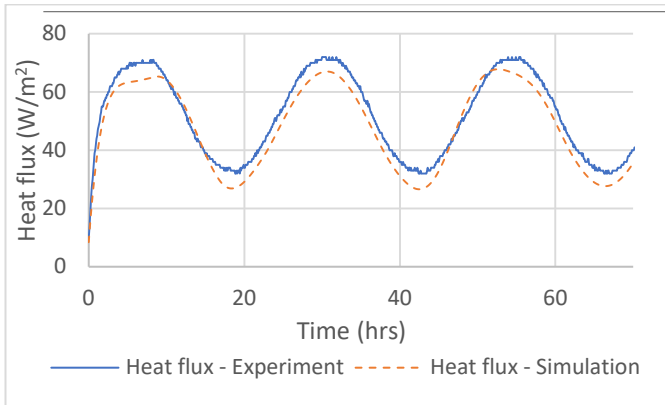
Figure 8. Comparison of experiment and simulation data of hot side surface temperature for solid wall

The disparity between the model and the experiment can be improved by further refining the mesh, using smaller time steps and by modelling the CC in full. Nonetheless, the obtained calibration index (Table 3) is within ASHRAE limits and therefore the model can be considered as calibrated. The EF index demonstrates that the data is within acceptable percentage of variation of below 5%. The higher the variation in the data lesser is the efficiency value. Parameters calculated for the solid wall using simulation data also appears to be very close to the measured data with an absolute error of 0.43 hours for phase lag and 0.42 cm for peak displacement and 0.51(-) for decrement factor.

Comparison of surface temperatures, heat flux and average air temperature in the cavity for the cavity wall shown in Figure 9 and Figure 10 revealed good agreement with an average relative error of 4.3 % (surface temperature), 2.8% (cavity air temperature) and 1.5% (heat flux). Improper fixing of the thermocouples on the hot side surface led to the discrepancies with CV of 20.1 (still within ASHARE limits) and EF of 0.9.

Table 3. Evaluation index

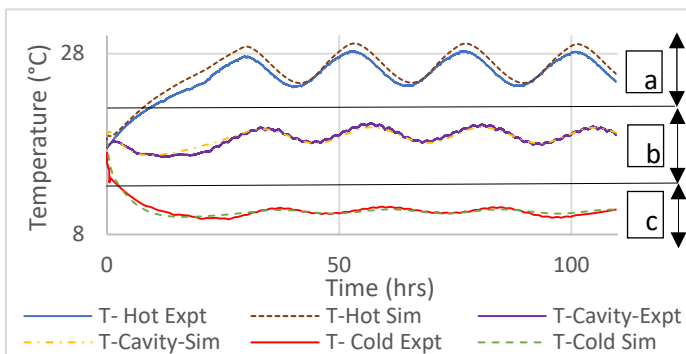|	Hot Surface (°C)	Cavity (°C)	Cold Surface (°C)	Heat Flux (W/m^2)
		Wall 1		
CV	12.9	N/A	24.9	20.1
EF	0.9	N/A	0.8	0.9
		Wall 2		
CV	20.1	18.3	15.3	8.6
EF	0.9	0.9	0.9	0.9

Figure 9. Comparison of experiment and simulation data for cavity wall (a) hot side surface temperature, (b) cavity air temperature and (c) cold side surface temperature
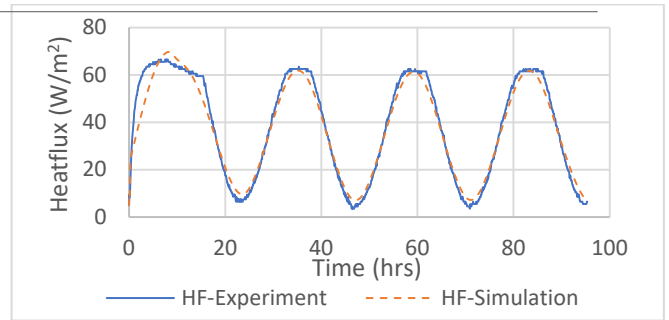

Figure 10. Comparison of experiment and simulation data of hot side surface temperature for cavity wall

6.3 Influence of wall configuration on the heat transfer coefficient in the Hotbox

Three-dimensional temperature distributions in the Hotbox chamber is illustrated for the solid wall in Figure 11a and cavity wall in Figure 11b. A greater temperature difference is observed for the HC in the solid wall simulation (Figure 11a) which has the lower thermal impedance and therefore greater rate of heat transfer (3.7 MJ/m^2 day) compared to cavity wall (2.1MJ/m^2 day).

Figure 12 shows the velocity profiles for the solid wall and cavity wall. The airflow regime in the enclosure is governed by the Rayleigh number (Ra),

$$Ra = \frac{g\beta c\mu(T_s - T_a)L^3}{k\vartheta^2} \qquad (13)$$

The average Ra calculated using the simulation data for the HC was found to be 2.17x10^8 for the solid wall model and 6.6x10^7 for the cavity wall. As per the literature, any internal low of Ra less than the order of 10^9 for vertical walls is considered to be laminar flow [25]. Thus, the flow regime in the Hotbox enclosure in both cases is laminar.

$$Nu = \frac{0.825 + 0.387(Ra)^{\frac{1}{6}}}{\left[1 + \left(\frac{0.492}{Pr}\right)^{\frac{9}{16}}\right]^{\frac{8}{27}}} \qquad (14)$$

$$h = \frac{Nu.K}{L} \qquad (15)$$

Another dimensionless parameter which characterized the heat transfer is the Nusselt's number (Nu), which is the dimensionless form of the convective heat transfer coefficient h. The average hot-side Nusselt's number was found to be 8.69 with the solid wall model and 7.1 for the cavity wall. The associated convective heat transfer coefficient are 2.5 W/m^{2}K and 3.4 W/m^{2}K for cavity wall and solid wall respectively. The higher the Nu value, the more effective the heat transfer coefficient. From the above results, it is found that the Nu and heat transfer coefficient in the case of the solid wall was higher than the cavity wall. This is because the rate of heat loss through the solid wall was greater. This resulted in a large temperature gradient shown in Figure 10a causing a higher heat transfer coefficient.
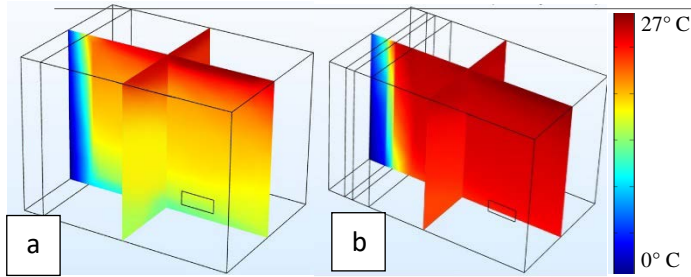
Figure 11. Temperature profile in the Hotbox with (a) solid wall (b) Cavity wall
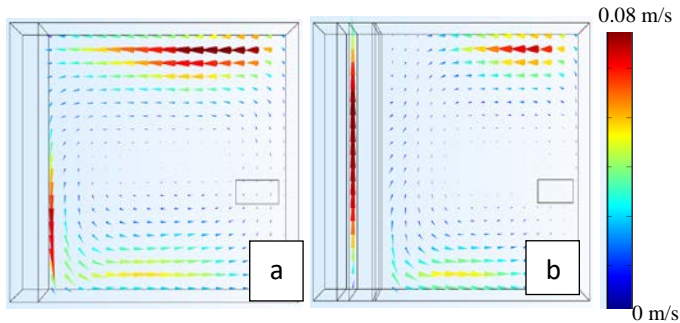

Figure 12. Velocity profile in the Hotbox with (a) solid wall (b) Cavity wall

7 CONCLUSION

The Conjugated Computational Fluid Dynamic models developed to simulate the Hotbox facility were found to be in good agreement with experimental results with an average CV of 18.9 and efficiency of 0.91 for the solid wall and average CV of 17.9, and efficiency of 0.9 for the cavity wall. The percentage error in both the cases was below 5 %. Improper fixing of thermocouples, experimental uncertainty and simplification of the modelling on the cold side can account for the discrepancy. Nevertheless, the results were within acceptable margins to verify the efficacy of the simulation models.

The parameters of phase lag, peak displacement, decrement factor and thermal impedance were evaluated using the measured surface temperatures and heat flux. It was found the wall with higher thickness and lower effective thermal diffusivity exhibits larger phase lag, peak displacement and lower decrement factor, which supports what is found in the literature. Here, the cavity wall experienced 2.9 times the phase lag and peak displacement of the solid wall and 1.6-time lower decrement factor. This translates to a delay in the peak load in the cavity wall of 4.5 hours when compared to the solid wall.

The numerical investigation suggests that for wall samples with lower thermal impedance and heat capacity, the heat transfer coefficients produced in the Hotbox will be higher, which exacerbates the problem of heat retention. In this case, the heat transfer coefficient value inside the hot box with the solid wall as a test specimen was found to be 26% higher than the cavity wall.

This presented methodology can be used for examining the influence of thermal mass in building walls, which is one of the main parameters considered in building energy regulation (BER) assessment along with insulation, U-value, air tightness, and fuel type. The verified model developed here will be used in future research to optimise the insulation thickness of various wall configurations. This will result in recommendations for building standards and guidelines for wall insulation retrofit which are more tailored to the existing wall type and environment.

References

[1] X. Cao, X. Dai, J. Liu, Building energy-consumption status worldwide and the state-of-the-art technologies for zero-energy buildings during the past decade, Energy and Buildings, 128 (2016) 198-213.
[2] A. Reilly, O. Kinnane, The impact of thermal mass on building energy consumption, Applied Energy, 198 (Supplement C) (2017) 108-121.
[3] K. Gregory, B. Moghtaderi, H. Sugo, A. Page, Effect of thermal mass on the thermal performance of various Australian residential constructions systems, Energy and Buildings, 40 (4) (2008) 459-465.
[4] A. Byrne, G. Byrne, A. Davies, A.J. Robinson, Transient and quasi-steady thermal behaviour of a building envelope due to retrofitted cavity wall and ceiling insulation, Energy and Buildings, 61 (2013) 356-365.
[5] X. Jin, X. Zhang, Y. Cao, G. Wang, Thermal performance evaluation of the wall using heat flux time lag and decrement factor, Energy and Buildings, 47 (Supplement C) (2012) 369-374.
[6] N.C. Balaji, M. Mani, B.V. Venkatarama Reddy, Dynamic thermal performance of conventional and alternative building wall envelopes, Journal of Building Engineering, 21 (2019) 373-395.
[7] R. Fathipour, A. Hadidi, Analytical solution for the study of time lag and decrement factor for building walls in climate of Iran, Energy, 134 (2017) 167-180.
[8] S.A. Al-Sanea, M.F. Zedan, S.N. Al-Hussain, Effect of thermal mass on performance of insulated building walls and the concept of energy savings potential, Applied Energy, 89 (1) (2012) 430-442.
[9] M. Ozel, Effect of insulation location on dynamic heat-transfer characteristics of building external walls and optimization of insulation thickness, Energy and Buildings, 72 (2014) 288-295.
[10] B. Rosti, A. Omidvar, N. Monghasemi, Optimum position and distribution of insulation layers for exterior walls of a building conditioned by earth-air heat exchanger, Applied Thermal Engineering, 163 (2019) 114362.
[11] H. Ramin, P. Hanafizadeh, M.A. Akhavan-Behabadi, Determination of optimum insulation thickness in different wall orientations and locations in Iran, Advances in Building Energy Research, 10 (2) (2016) 149-171.
[12] S.A. Al-Sanea, M.F. Zedan, Optimum insulation thickness for building walls in a hot-dry climate, International Journal of Ambient Energy, 23 (3) (2002) 115-126.
[13] T. Tzoulis, K.J. Kontoleon, Thermal Behaviour of Concrete Walls Around all Cardinal Orientations and Optimal Thickness of Insulation from an Economic Point of View, Procedia Environmental Sciences, 38 (2017) 381-388.
[14] P.M. Toure, Y. Dieye, P.M. Gueye, V. Sambou, S. Bodian, S. Tiguampo, Experimental determination of time lag and decrement factor, Case Studies in Construction Materials, 11 (2019) e00298.
[15] C. Sun, S. Shu, G. Ding, X. Zhang, X. Hu, Investigation of time lags and decrement factors for different building outside temperatures, Energy and Buildings, 61 (2013) 1-7.
[16] K. Ulgen, Experimental and theoretical investigation of effects of wall's thermophysical properties on time lag and decrement factor, Energy and Buildings, 34 (3) (2002) 273-278.
[17] M.M. Vijayalakshmi, E. Natarajan, V. Shanmugasundaram, Thermal behaviour of building wall elements, Journal of Applied Sciences, 6 (15) (2006) 3128-3133.
[18] K. Ulgen, Experimental and theoretical investigation of effects of wall'sthermophysical properties on time lag and decrement factor, Energy and Buildings, 34 (2002) 273-278.
[19] S.M.A. Bekkouche, T. Benouaz, M.K. Cherier, M. Hamdani, M.R. Yaiche, N. Benamrane, Thermal resistances of air in cavity walls and their effect upon the thermal insulation performance, International Journal of Energy and Environment, 4 (3) (2013) 459-466.
[20] C. Ahern, P. Griffiths, M. O'Flaherty, State of the Irish housing stock— Modelling the heat losses of Ireland's existing detached rural housing stock & estimating the benefit of thermal retrofit measures on this stock, 2013.
[21] A. Guideline, 14 (2014). ASHRAE Guideline 14-2014 for Measurement of Energy and Demand Savings, American Society of Heating, Refrigeration and Air Conditioning Engineers, Atlanta, GA.
[22] L. Evangelisti, C. Guattari, P. Gori, F. Asdrubali, Assessment of equivalent thermal properties of multilayer building walls coupling simulations and experimental measurements, Building and Environment, 127 (2018) 77-85.
[23] G.E.C. K.W. Childs, E.L Bales, Thermal Mass Assessment - An Explanation of the Mechanism by Which Building Mass Influences Heating and Cooling Energy Requirment, in, 1983.
[24] A. Byrne, G. Byrne, A. Robinson, Compact facility for testing steady and transient thermal performanceof building walls, Energy and Buildings, 152 (2017) 602-614.
[25] Y.A. Cengel, S. Klein, W. Beckman, Heat transfer: a practical approach, McGraw-Hill New York, 1998.